Structure transfer between a polymer melt and the solid state. Investigation of the nanostructure evolution in oriented polyethylene by means of continuous X-ray scattering*

Norbert Stribeck[1]†, Peter Bösecke[2], Rüdiger Bayer[3],
Armando Almendarez Camarillo[1]

[1]Institut für Technische und Makromolekulare Chemie, Universität Hamburg, Bundesstr. 45, 20146 Hamburg, Germany
[2]Institut für Werkstofftechnik, Universität GH Kassel, Mönchebergstrasse 3, 34125 Kassel, Germany
[3]ESRF, 6 rue Jules Horowitz, B.P. 220, 38043 Grenoble Cedex 9, France

Progress in Colloid and Polymer Science (2005), *in print*

Abstract

During the melting and crystallization of uniaxially oriented polyethylene small-angle X-ray scattering (SAXS) and wide-angle X-ray scattering (WAXS) patterns are recorded simultaneously and continuously, i.e. with high signal-to-noise ratio and a time resolution of 7 s. The multidimensional chord distribution function (CDF) is computed from each of the SAXS patterns and visualises the nanodomain structure of the material in physical space. Thus without application of a model a detailed and continuous multidimensional stream of data is obtained that reveals the mechanisms which govern melting and crystallization in the material studied. Finally the CDF is semi-quantitatively analysed as a function of the temperature programme.

We find that swarms of small crystalline blocks which are observed during the heating of the injection moulded rods are melting earlier than the extended lamellae. Directly after the last lamellae have vanished we quench to a crystallization temperature. No formation of blocky crystals is observed. Instead, before the beginning of crystallization, a mesophase separation into disentangled and entangled regions is indicated. Moreover, row structures of nuclei are observed coming and going. As long as these rows are oriented in fibre direction, the orientational memory of the melt is not erased. Crystallization starts in disentangled bundles of chain segments at the tips of knots (entanglement strands). Fast and continuous lamellar growth is observed. Most of the lamellae are positioned at random. Correlations between lamellae are limited to twins which are formed when lamellae grow at both ends of the same entanglement strand. Thereafter slow thickness growth of lamellae is observed, and in twins this growth is directed outwardly, away from the entanglement-rich amorphous zone between them. Only during this period the wide-angle X-ray scattering (WAXS) exhibits an increasing orientation of the crystals. At a high undercooling or after there is no space for lamellae any more, secondary crystals (blocks) are formed that are unoriented but placed in such a manner that correlations among them are high both in longitudinal and transversal direction. **Keywords** Fibers, Polyethylene, SAXS, Crystallization, Melting,

*Dedicated to Prof. Dr. Wilhelm Ruland on the occasion of his 80th birthday

†Corresponding author. Phone: +49 40 42838 3615, FAX: +49 40 42838 6008,
e-mail: Norbert.Stribeck@desy.de

1 Introduction

The mechanisms of structure transfer which are the basis of polymer crystallization have been studied in polymer science for several decades. Since industry has returned to the tailoring of bulk polymer materials, this field is back in the focus of scientific interest [1–8]. Nevertheless, the views concerning the nanostructure evolution are still conflicting, because the experimental data collected so far are still incomplete. In this paper we propose and exercise a method that appears apt to narrow the mentioned gap and is resting on both in-situ experiments with high time resolution using oriented materials, and an advanced technique of data analysis.

Using imaging methods like atomic force microscopy (AFM) or scanning near-field optical microscopy (SNOM) it appears very difficult to in-situ monitor a structure transfer process executed under technical conditions with sufficient resolution corresponding to both time and space [9–11]. Utilising X-ray scattering, such experiments are possible, but the recorded data require mathematical evaluation, as long as it is not considered to apply simplified notions. Unfortunately a mathematical treatment is still frequently avoided, and thus the present state of science in the field of small-angle X-ray scattering (SAXS) is similar to the state of solid-state NMR before the multidimensional NMR was invented.

Since several years one of us is developing automated data evaluation methods for the SAXS aiming at the investigation of nanostructure evolution processes [12–15]. Fundamental with respect to this development is the principle of late modelling which, for the field of SAXS and nanostructure analysis, has been pointed out early in the work of Ruland [16–21]. According to this principle the interesting information concerning the structure is first extracted from the raw data, then visualised after an appropriate Fourier transformation, before, as the final step, modelling comes into play.

Such kind of investigations make substantially higher demands on the experiment than common SAXS studies carried out at synchrotrons with two-dimensional (2D) detectors. If the only goal is to document that a peak is emerging and moving, a SAXS setup at a less-advanced synchrotron, a typical sample-to-detector distance of 2 m and a small detector with few pixels is adequate. If a Fourier analysis is the aim, it is no longer sufficient to be able to recognise a peak close to the beam stop, the position of that equals a long period of 100 nm. Then, additionally information from the USAXS region is required, which has to be recorded with both high signal-to-noise (S/N) ratio and high spatial resolution on a large detector positioned in typical USAXS distance.

If, today, we combine sufficiently equipped synchrotron radiation facilities with both an advanced concept of analytics for the investigation of oriented polymer materials, it becomes possible to study the processes of structure transfer in two or three dimensions of physical space. Figuratively, we no longer interpret the fringe structure of a hologram, but shine light on it and describe the image that is flashing up. Recently we have already reported results of corresponding crystallization experiments [22–24], which have been carried out with a time resolution of 2 min at the Hamburg Synchrotron Laboratory (HASYLAB). Because of the coarse time pattern some basic questions concerning the mechanisms of melting and crystallization remained unanswered. We found, for example, not only lamellar crystals, but also distorted lattices from block-shaped ones, which are much less extended than the lamellae. Nevertheless, we were not able to enlighten the genesis of the latter. Alike we observed in our high S/N-data row structure nuclei before the first lamellae showed up; two minutes later there was nothing but a crowd of oriented lamellae placed at random positions. We postulated that the statistical placement should have been preceeded by a regular and long ranging “shish kebab” [25] structure. Now we present the results from an extended series of experiments that have been recorded at the European Synchrotron Radiation Facility (ESRF) in Grenoble, where time resolution was

increased to 7 s at even higher S/N-ratio as compared to the earlier studies. Utilising such a fine time pattern at high data quality we are entering the new field of continuous and multidimensional investigation of nanostructure evolution, and thus achieve new vistas concerning the mechanisms that are governing the processing of polymer materials, as has already been pointed out in a short communication [26].

In order to record such data streams, a powerful X-ray source and two modern two-dimensional (2D) detectors are required. The concept of scattering pattern analysis developed by us utilises methods of image processing that have successfully been applied in medical technology for years. Combined we obtain a detailed image in physical space of the correlations among the surfaces of the crystalline domains. This image is the multidimensional chord distribution function (CDF) [14, 27, 28].

In particular during the period of nascent nanostructure the CDF is a favourable tool, because it perfectly discriminates the emerging structure (correlation peaks in the CDF) from the chaos (CDF vanishing everywhere). On the other hand, the interpretation of such weak pre-crystalline structures never seen before appears to be susceptible to misinterpretation to a considerable extent.

As here we report results of an in-situ study of polyethylene crystallization, we continue a series of papers [29–31] aiming at the advance of understanding structure transfer between a polymer melt and the solid state.

2 Experimental

Highly oriented polyethylene (PE) rods are prepared from commercial material, cautiously melt–annealed in a furnace, and finally crystallized in the synchrotron beam of an ultra small–angle X–ray scattering (USAXS) beam line. In the majority of the experiments orientation is preserved, although the nanostructure itself changes completely.

Commercial high-density, low-branched Ziegler-Natta type polyethylene is used for our experiments (Lupolen 6021 D, BASF, M_W=182 kg/mol, M_n=25 kg/mol, density 0.962 g/cm^3, melt index 0.2). In order to achieve high orientation, an equilibrated, low–temperature melt (160°C) is injected into a cold mold. Maximum mold pressure is 444 MPa and final mold pressure 336 MPa after 180 s. In the differential scanning calorimetry (DSC) the material exhibits bimodal melting with peak maxima at 131°C and 141°C.

As a result of this high-pressure injection-moulding (HPIM) process, rods of 10 cm length and a diameter of 6 mm are obtained. Inspection by the eye exhibits a core–shell structure with a core diameter of 2.5 mm. Samples for the present investigation are sectioned [32] from the shell of the rod using a low–speed diamond saw. In tests carried out during previous experiments [32] we ascertained fibre symmetry by comparing the scattering patterns before and after turning the samples by 90° about fibre axis and finding no difference.

The experiments are performed in the synchrotron beam line ID02 [33] of ESRF. The wavelength of the X-ray beam is 0.1 nm. USAXS images are collected by a two-dimensional position sensitive XRII–FReLoN (“X-Ray Image Intensifier, Fast Readout, Low Noise”) CCD detector developed at ESRF (driven in1024×1024 pixel mode of each $0.164 \times 0.164\,\mathrm{mm}^2$, 14 bit resolution). The sample–to–detector distance is set to 10 m.

Wide-angle X-Ray scattering (WAXS) is simultaneously recorded using a MCP-Sensicam CCD detector positioned [34, 35] at a short distance of the sample.

Samples of 2 mm thickness are mounted in a Mettler-Toledo FP82HT hot stage and subjected to a temperature programme. Temperature is measured using a separate thermo couple being in direct contact with the sample. USAXS exposure is varied during the experiment between 0.1 s and 3 s in order to always use the full linear range of the detector, i.e. in every image the most intense pixel is exposed to about 14000 counts. The incident beam is attenuated by a factor of 10 in order

to keep the exposure in a reasonable range with respect to the available timers and counters. A minimum cycle time of 7 s between two snapshots provides for both control of exposure and data storage (4 s) of single snapshots. We use to start with an exposure of 0.3 s as soon as the material is reaching a temperature of 120°C, then decrease it to 0.1 s up to the moment when most of the material is melting. Thereafter we instantly increase to 3 s and finally slowly adjust to lower exposure. The CDFs presented in Figure 2 are computed from scattering patterns which have been exposed for 3 s each.

The flexible concept of a general experiment control by small programme modules under Linux which communicate via pipes has been a crucial prerequisite for the ad-hoc implementation of the dynamic exposure control.

3 Data evaluation

A major problem concerning time-resolved 2D-experiments is the sifting and evaluation of the data flood. In 3 days we have accumulated 30 GB of data. In order to pre-evaluate the huge amount of scattering patterns we have adapted our evaluation programme to the actual local experimental conditions and have added a parameter tracking system. As a result, the most frequent action of the user is nothing but a mouse click that confirms the computed proposal concerning centre and alignment of the pattern. Utilising this procedure the pre-evaluation can be carried out in tolerable time. Thereafter the scattering images belonging to a series are automatically transformed to the multi-dimensional CDF of a nanostructured sample with fibre symmetry [14, 22, 32].

For the purpose of visualisation the CDFs are, in general, plotted in a logarithmic intensity scale. The obvious method to handle negative values is described upon request. For the plot an upper level of interest in the CDF is scaled to a value of 100. A mask eliminates all values below 0.1. The logarithm is taken. An inverted copy of the CDF is treated the same way and re-inverted. Both partial surfaces match and, "glued together", yield a continuous 3D surface in a logarithmic scale.

Concerning the next step, i.e. sifting of the CDF results, a manual survey has proven inapplicable. In order to take advantage of the continuous multi-dimensional data stream, adapted presentation tools have to be built in order to become able first to comprehend the dynamics of the process, and, second to properly describe it.

Therefore we have programmed animation tools. In the most simple case we choose a fixed viewpoint and scale, load one CDF after another from the hard disk, and display it on the computer screen. Such an animation cannot be controlled by the user, the built-in display quality of our data evaluation language pv-wave [36] is insufficient for our purpose, and we can only watch single 3D functions viewed from a single viewpoint. In order to improve the practical value of the animation we have rendered the data from each snapshot (USAXS, WAXS, CDF from two viewpoints) using a ray-tracing programme (PoVRay 3.1), have combined them in a composite image and, in the final step, have merged the series of composite images to make it a movie. Format conversions and image composition are carried out by the modules of the ImageMagick package. The movie is generated by transcode.

Ultimately, as the control functions of the programme mplayer are used to replay the movies, the essential phases and processes of nanostructure evolution become evident. All the programmes mentioned (except for pv-wave) are free software and have been developed by the community of Linux programmers.

4 The CDF of distorted structures

The structure evaluation method used in this report extracts the information on the samples nanostructure (i.e. a topology $\rho(\mathbf{r}) \in \left[\rho_{\text{cryst}}, \rho_{\text{amorph}}\right]$ of phases with distinct densities) from two-dimensional (2D) SAXS patterns with fibre symmetry. The CDF $z(\mathbf{r})$ is an "edge-enhanced autocorrelation function" — the auto-

correlation of the gradient $\nabla\rho(\mathbf{r})$, or the Laplacian $\Delta\left(\rho^{*2}(\mathbf{r})\right)$ of Vonk's multidimensional correlation function [37] $\rho^{*2}(\mathbf{r})$. It shows peaks where ever there are domain surface contacts between domains in $\rho(\mathbf{r})$ and its displaced ghost as a function of ghost displacement.

Thus, compared to the correlation function $\rho^{*2}(\mathbf{r})$, the effect of the CDF is "edge enhancement", if we apply the terminology of the field of digital image processing. This means that for multi-phase systems the interpretation of the CDF is obvious, but from its mathematical definition it is not restricted to such systems and, therefore, can be applied to deliberate distributions of density $\rho(\mathbf{r})$ in space. However, in the latter case its interpretation may be difficult or even impossible.

If, in the sequel, we take the chance to as well interpret the distorted structures observed in the CDF of the cool polymer melt, then we apply a similar method of edge enhancement as astronomy when it is using the very Laplacian operator [38, 39], in order to visualise details in photographic images of the universe. Similar to our case, the mentioned images cannot be described by a small number of discrete phases. Nevertheless, the mathematical operator acts edge-enhancing and visualises details, which are difficult to find in the raw data. Admittedly, the interpretation of such details is to some extent speculative. On the other hand, there are several reasons encouraging us to publish our data and our interpretation:

1. We are reproducing the structural details in all experiments on this material during the last four years – and now even on a totally different instrument.

2. We are able to erase the observed details details in the CDF by heating the melt to a higher temperature.

3. The danger that the features are artifacts which are generated by Fourier transformation of noisy data is much smaller now because of the very good S/N-ratio achieved at the ESRF beam line. Single adulterated scattering patterns are easily detected in the extended series due to the short cycle time between snapshots.

4. The reported measurements with high time resolution exhibit for the first time that an initially monotonous CDF feature first changes to form discrete peaks (i.e. a mesophase), before crystallization is starting.

5 Results

5.1 From the injected rod to the oriented melt

The nanostructure as reflected in the CDF. Our experiments start from highly oriented, HPIM-PE rods which, in a first step, are slowly melted. In contrast to an earlier paper [32] it now has become possible to record the structure transfer with high accuracy and quasi-continuously. Figure 1 shows three phases during the heating.

The presented CDF of the melting semicrystalline material describes the correlations among domain surfaces. In the present paper the functions are always scaled to a constant maximum amplitude, because we are focusing on the investigation of topology variations. In the left column (Figure 1a) the typical triangular peaks of lamellar domains are observed with their surface normals oriented parallel to the fibre axis, as was already reported in previous work [32].

Figure 1b demonstrates the transitional stage between solid and melt. The corresponding movie clearly exhibits the regression of the lamellar structure which is accompanied by the emerging of a novel kind of structure, which is characterised by a narrow negative ridge on the meridian of the CDF. We address this feature by a row structure . It is worth to be noted that a "shish" made from a bundle of straightly extended chains would be characterised by two close, narrow and positive ridges extending on both sides of the meridian. The negative ridge can only be explained by a modulation of electron density, and the observed

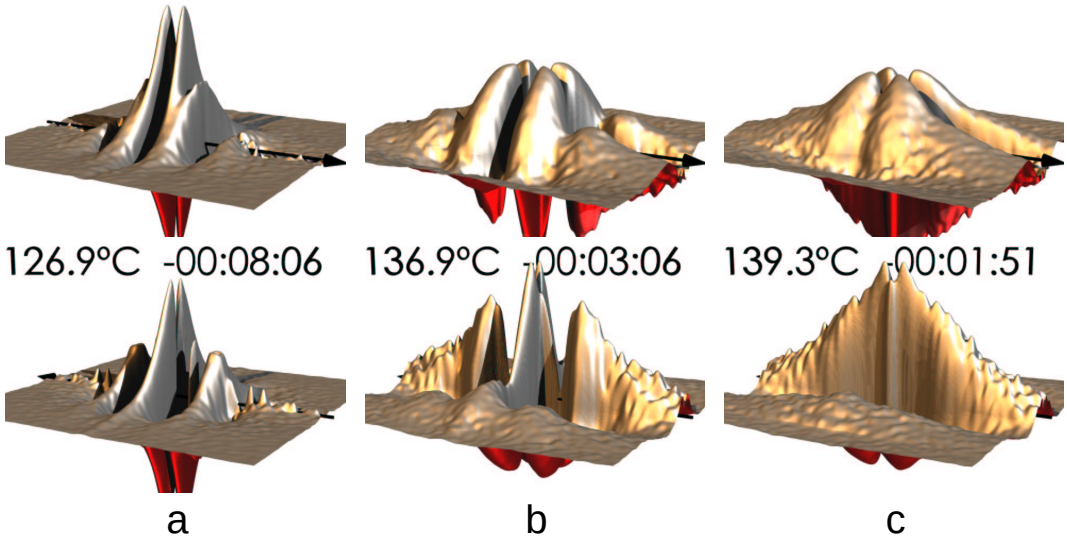

Figure 1: Heating of HPIM–PE. The images show the CDF in a logarithmic intensity scale watched from a top viewpoint (top) and a bottom viewpoint (bottom), respectively. The fibre axis (meridian) is indicated by an arrow in the base plane. The clips represent an area of 300 nm×300 nm. Times are computed with respect to the moment of quenching the melt.

shape of the peak indicates a peculiar probability distribution of long periods according to an exponential fall off.

Outside the meridian we, additionally, observe strong and diffuse positive regions that, in the course of melting, are more and more veiling the lamellar peaks on the top face of the CDF. Fortunately the CDF shows a second and clear feature related to lamellae-shaped domains that is not veiled during the process of melting. If we turn the CDF upside down (Figure 1b, bottom) the self-correlation peak of a lamellar system (cf. [14], Figure 9) is found on the equator. In the plot it is almost looking like a triangle. During the melting process the width of this triangle is narrowing continuously. Thus the lamellae are melting continuously from their edges. There is little evidence of a subdivision process into blocks.

In a previous paper [22] we reported the results of a survey carried out at HASYLAB. A few minutes before melting a block structure (i.e. floes in planes with their normal parallel to the fibre direction) had sometimes been observed. Because of the outdated detector at beam line BW4 the evolution of this block structure could not be studied. In the experiments from the ESRF presented here we use only 10% of the incident intensity, adjust to a tenfold S/N–ratio and a 15fold time resolution. Again we sometimes find modulations of the triangular peaks that indicate the presence of arranged blocks. Nevertheless, now the continuous stream of data reveals that such block structures vanish before the lamellae themselves start to melt, and that the observed blocks are less stable than the lamellae.

Admittedly, there is a feature observed during melting that we first took for an indication of a block structure during melting when we sifted through the images one by one. It is related to a negative ridge subdivided in three parts (Figure 1b bottom) that is extending parallel to the meridian in a distance of 200 nm. Observing the corresponding videos it becomes clear that this feature does not grow in phase with the melting of the lamellae. Instead, it is correlated both to the four diffuse positive domain peaks that are veiling the lamellar triangles (Figure 1b, top) and the sharp row structure on the meridian (Figure 1b,

bottom). Moreover, the discussed negative ridge is found outside the range of lamellae extension, and thus can hardly indicate a decomposition of lamellae.

The row structure. At the end of the melting we still observe a small bulge in equatorial direction indicating the presence of crystallites ("kebab"). Just when this bulge has vanished, the discrete WAXS has vanished as well. Nevertheless, the row structure is surviving the melting of the crystallites (Figure 1c). In this phase of the melting there is no preferential distance between the row nuclei, else the meridional triangle should be subdivided into a sequence of peaks. If, moreover, the nuclei would show a rather uniform height (in fibre direction), then, in addition, we would expect discrete peaks pointing upwards on the meridian (in Figure 1c, top). However, there we only find a diffuse positive region extending far out into space. The structural feature behind this CDF feature cannot be explained by the row structure itself. So, although this is only a poor approximation of structure with respect to the observed regime of a cool melt, let us use the notion of domains and answer the question, in which simple case we would observe a positive region in the CDF. The most simple explanation is some weak segregation in the melt, and in this case the positive signal $z(\mathbf{r}')$ at some displacement $\mathbf{r}'$ would measure the probability of finding a chord crossing a "homogeneous" domain of length and direction given by $\mathbf{r}'$. Prerequisite is that there are no correlations among the regions of segregation. The structure and its evolution shows that such segregation-domains are associated to the row structure and reach out into space. Therefore we call them "row structure associated domains", RADs. We recognise that the diffuse positive regions in the CDF are characterising a volume in correlation space that is governed by such RADs.

In Figure 1c, top, an indentation on the equator reflects an aspect of memory concerning the lamellar structure of the precursor material: With respect to the beginning of a RAD its end is preferentially found in a distance A along fibre direction. A shrinks during the progress of melting, and the longitudinal extension of the RADs becomes more and more statistical. Finally, in the melt there is no preferential RAD extension any more. However, let us go back and, again, compare this image to Figure 1b, top, where still a much stronger modulation of the RAD structure is observed. There a majority of the RADs is still restricted to regions whose extensions in fibre direction are given by the average amorphous thickness, A, in the lamellae stacks of the precursor injection moulded rod.

The ultimate orientation preserving structure of the melt. Figure 2 shows some of the CDFs recorded close to the melting point. Although the intensity of the row structure is decreasing by two orders of magnitude, its principal shape remains similar for a considerable period when the melt-annealing temperature of 140°C is reached (Figure 2a) (recent test measurements show that even after 20 min at 140°C the basic topology remains unchanged). Nevertheless, during the period of constant temperature one feature of the topology is vanishing (Figure 2b). It is related to the melting of the last lamellae, and the corresponding change of the diffuse scattering can hardly be detected during the course of the experiment.

Because during our experiments we expected the ultimate orientation preserving structure to be destroyed after a long period of melt-annealing, we have only kept the samples at the melt-annealing temperature for 2 min, and thus sometimes have not reached the pure ultimate orientation preserving structure of the melt that is shown in Figure 2b. In the other experiments we have got stuck in a densely populated row structure with a few isolated lamellae persisting (Figure 2a). This difference has a consequence on the following process of crystallization that is reported in section "Crystallization from the oriented melt".

The ultimate orientation preserving structure is a sparse row structure (Figure 2b) and exhibits on the meridian of the CDF a statistical ensemble of rows. Each row is made from nuclei of varying

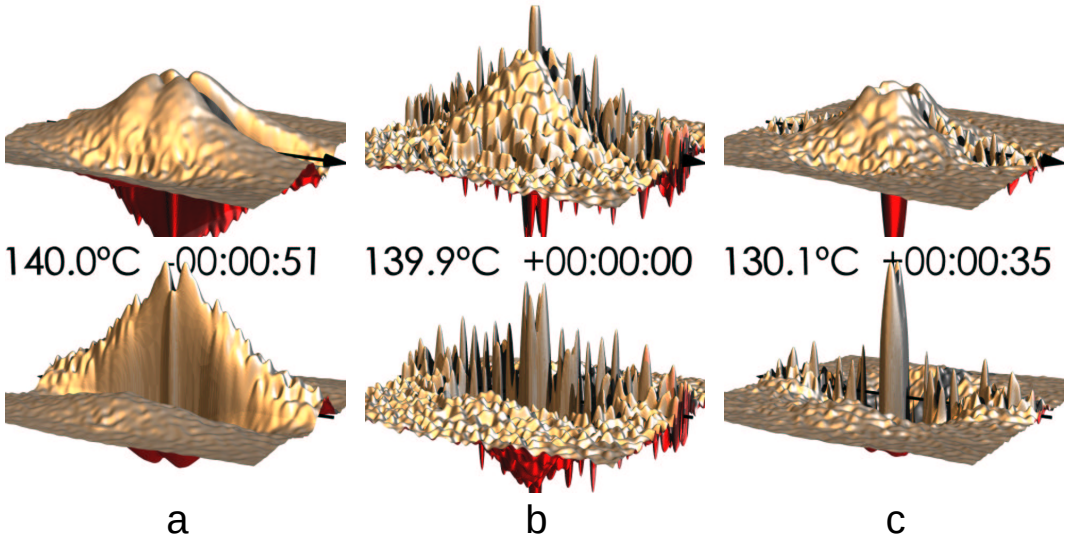

Figure 2: The last phase of HPIM–PE melting and the beginning of quenching. The images show the CDF in a logarithmic intensity scale watched from a top viewpoint (top) and a bottom viewpoint (bottom), respectively. The fibre axis (meridian) is indicated by an arrow in the base plane. The clips represent an area of 300 nm×300 nm. Times are computed with respect to the moment of quenching the melt

thickness but well-defined long period, and during the period of melt-annealing the thicknesses of the nuclei become more homogeneous, so that now positive *and* negative peaks show up, as is expected for a simple one-dimensional lattice of homogeneous nuclei. In the raw data scattering pattern the corresponding layer line is not directly observed, but the interference function (computed by projecting the scattering data and applying the Laplacian in reciprocal space) shows the feature. In addition, on the top face of the CDF we still observe the continuous and diffuse positive peak of pyramid shape that is characterising a very broad distribution of RADs (with the most probable chord of the RADs being an infinitesimally short one).

In the figure this pyramid is already slightly structured, and after it decomposes into single peaks of similar strength as those characterising the oriented row structure, an isotropic phase is observed during the following crystallization process. The orientation memory is lost. Nevertheless, as long as the oriented row structure is still observed on the meridian, the result of the following crystallization is a two-component material comprising both a highly oriented structure and an isotropic one [22].

In earlier work [32] on the melting of HPIM–PE we have reported discrete and regular undulations on the row structure ridge in the CDF based on experiments at HASYLAB. Because of the long exposure required in Hamburg we that time have integrated the pulsating row structure for 2 min, and this integration results in the undulations formerly observed.

In a short communication [26] the results concerning the structure formation during cooling and before the first crystallites show up are presented in combined SAXS/WAXS patterns and sketches of the nanostructure. Here we only summarise the results.

Now quenching the sparse row structure to the crystallization temperature we immediately observe a novel, now less extended nanostructure of RADs, from which a lamellar structure will grow that, again, is highly oriented. Due to the high time resolution we observe that the row structure itself is only a latent one. In our previous study

[22] based on data accumulated with a coarse time resolution we had perpetuated the common notion that from a static row structure or a "shish" (bundle of extended chains) one-dimensional lattices of lamellae should have formed which (during the next two minutes needed for exposure) should have been overgrown by many secondary lamellae poured in between. Now we observe that the correlations among most of the nuclei stringed like beads on a chain are subjected to atrophy, and we speculate that the creation of a primary nucleus is going along with the generation of a harmonic sequence of only latent secondary nuclei that extend along the preferential direction of the polymer chains. A second possible explanation would be to assume that all the nuclei are converted into crystals, but that the crystal growth itself is destroying the correlated arrangement among them.

Discussion of the RAD structure. Up to this point we have described the development of the CDF in the vicinity of the melting point without modelling the RADs. We have observed that the lamellae do not disintegrate into blocks upon melting. Moreover we have found a nanostructure emerging that is made from a row structure and row-structure associated domains. What kind of notions can we associate to these RADs? Certainly there must be some contrast in electron density between the RADs and a matrix phase in the melt.

We assume that the contrast observed is caused from a different degree of chain entanglement what the RADs and the matrix phase is concerned. If we write the pyramid shaped positive peak in the CDF as a chord distribution, $f_o\,(r_{12}, r_3)$, in correlation space described by the transverse coordinate r_{12} and the longitudinal coordinate r_3, the height f_0 may be associated to the probability to find the other end of the RAD chord at (r_{12}, r_3), and the identification of RADs with strands of entanglements or knots appears to be reasonable. Two observations make us assume that the RADs are entanglement strands and as such the precursors of the amorphous phase but not pre-crystals (bundles, nuclei). Firstly, there is another feature (the row structure) that appears to be related to nuclei in the melt. Secondly, as crystallization is starting later on, not the crystalline layers but the amorphous gaps are emerging from the RADs.

In the oriented melt the RAD peak is a pyramid with its maximum in the origin of correlation space. So most of the RADs are single entanglements. Nevertheless, some of the RADs reach out far into space and may be identified by the knot zones of the entangled network [30, 31]. In the most extended ultimate melt structure at the end of the melt-annealing period (Figure 2b) the extension of the region governed by the RADs is more than 300 nm in longitudinal direction and 130 nm in transverse direction.

At each side of the central column in Figure 2 more solidified states of the melt are shown. Both in Figure 2a and in Figure 2c there is no pyramid peak. Instead, the positive peak of the RADs appears indented both along the meridian and the equator. A "sofa cushion peak" exhibiting four lappets has replaced the pyramid. Thus at this stage of the crystallization process a domain structure is, for the first time undoubtedly observed. We interpret the observed change of the CDF from the pyramid to a sofa cushion shape as a mesophase separation process causing the merging of single entanglements and other RADs into an ensemble of better defined RADs of preferential size and orientation. The most probable RAD no longer is a single entanglement, but a strand extending under an oblique angle with respect to the fibre direction (meridian). As a result of melt solidification thus we observe a condensation of entanglements, and a mesophase separation into entanglement- or knot-strands [30, 31] and bundles [8] takes place. As a function of increasing solidification the relative probability of long-ranging strands is decreasing. It remains unanswered, if this effect is caused from a compression of existing knot strands or from the precipitation of additional and less extended strands.

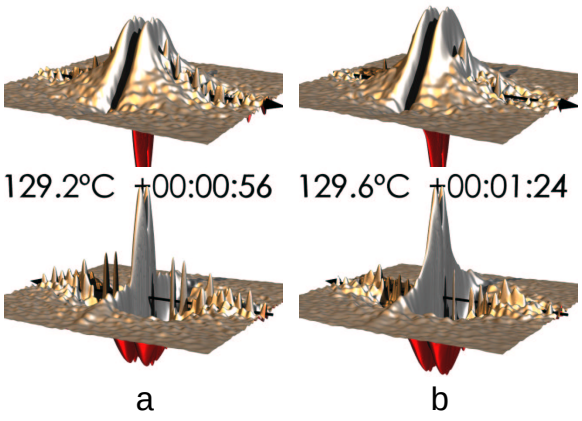

Figure 3: Oriented crystallization of PE from the RAD structure

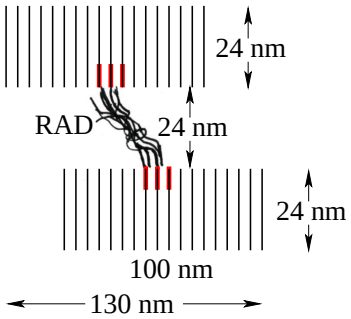

Figure 4: Isothermal crystallization of PE at 130°C. Sketch of the characteristic nanostructure of a lamellar twin as indicated by the CDF. The entity is showing two crystalline and one amorphous layer of almost equal thickness. At the tips of the RADs (row nuclei associated structure) primary nuclei are indicated, from which the twin lamellae have been grown

5.2 Crystallization from the oriented melt

RADs and crystallization. Only 20 s after the RAD pyramid has been converted into the mentioned sofa cushion shape we observe the first crystals in the CDF (Figure 3a). In the top view we detect the corresponding tip of the peak on the meridian exactly between two lappets of the RAD structure. Because of the strong RAD peaks we are unable to discriminate the shape of the crystals, but in the bottom view beneath we observe on the equator the sharp self-correlation ridge of lamellae on the equator sitting on the background of the RAD "sofa cushion". In comparison to the block shaped nuclei on the meridian that are still present at this early stage of crystallization it becomes clear that the first lamellae are not preceeded by ensembles of blocks arranged on planes. Shortly after that (Figure 3b) the strength of the RAD feature on the equator has decreased, and the extended lamellae are now very clear. Inspecting the RAD peaks we observe that the lappets have become compressed and converted into thickness distributions of amorphous layers.

Primary crystallization of our polyethylene material is finished after the crystal lamellae have formed. We do not observe series of layer peaks that would be typical for a lattice of alternating crystalline and amorphous layers, and the only observed quartet of peaks related to non-crystalline structures is readily explained by a mechanism, in which crystalline layers are formed at both ends of the same entanglement strand (Figure 4). We can discriminate the amorphous layers from the crystalline ones, because the maxima of their triangular peaks are displaced off the meridian. In the structure-ghost construction of CDF peaks this displacement is additionally required in order to perfectly match the bottom surface of one crystalline lamella on the top surface of its related twin. Because during the processing this shift is continuously emerging from the lateral tilt of the most probable RAD, the RADs appear to have a chaperoning function for the formation of amorphous layers between correlated twin lamellae.

Bundles and knots, blocks and lamellae. In summary, before the start of crystallization we observe a phase separation into bundles and knots (RADs). To us it appears most probable that the phase separation is driven by the formation of bundles from parallelised polymer chains which are not yet crystalline, but crystallizable. A force generated by bundle growth might then cause the

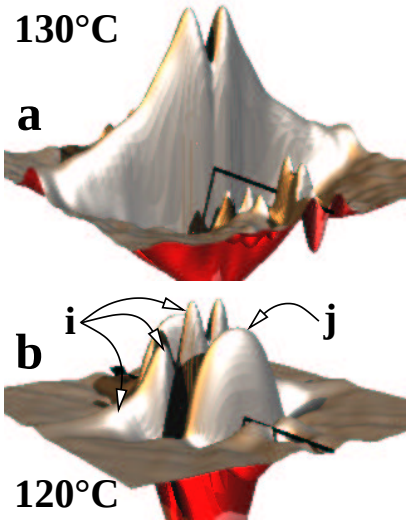

Figure 5: Lamellae **(a)** and a plane tiled with blocks **(b)** are clearly discriminated in the CDF. View of the bottom face of the CDF in the range $|r_{12}|, |r_3| \leq 150$ nm. The r_3–direction (meridian) is indicated by an arrow in the base plane. Both images show the structure during isothermal crystallization of PE 90 s after quenching

entanglement strands to become compressed and tilted. Because of the relatively low molecular mass of our material the knots do not percolate [30], and the crystallizable bundle phase is forming the matrix in the cool melt. Only if we were willing to define the average distance between the knots in transversal direction as some block extension, then the crystallization could be said to be preceeded by a block structure.

Crystal nuclei are supposed to predominantly emerge from the interface between knots and bundles, and this proposed mechanism is able to explain the observed association between the entanglement strands and the structure of row nuclei. The generation of a primary nucleus at an interface appears to induce the generation of a row of secondary nuclei, the whole row being a latent nanostructure only. Crystallization at low undercooling causes the first crystallites to rapidly and continuously grow into lamellar shape. Most probably during this process knots are circumvented and enclosed in the crystalline domain.

During crystallization at high undercooling we find that after a short period of time most of the domains are no longer lamellae. Instead, we observe planes tiled with blocky crystals (Figure 5). The two CDFs in the figure show the situation 90 s after the start of isothermal crystallization at 130°C (Figure 5a) and 120°C (Figure 5b), respectively. The differences of the nanostructure are clear. At 130°C we observe on the equator a strong intensity ridge that is decreasing monotonously as a function of distance (triangular peak). The observed discontinuity in the centre is an artifact resulting from the automatic data evaluation (background scattering correction). Crystallizing at 120°C, the ridge is clearly modulated (i) and thus reveals oriented planes full of blocky crystals. Moreover, on the meridian we always observe a strong long period peak (j) emerging, as soon as blocks are becoming the predominant crystalline feature. This shows that only the blocks, i.e. the secondary crystallites, are seeking strong correlations (short-range order, lattice) with other domains, whereas the primary lamellae occupy volume without any relation to their neighbours (random car parking process) [22–24] — as long as the already mentioned formation of twins is disregarded.

Nanostructure evolution visualised in movies. The dynamics of nanostructure evolution during the crystallization as a function of different temperature profiles are most clearly visualised in sequences of 3D representations of the CDF that are collected in movies (http://www.chemie.uni-hamburg.de/tmc/stribeck/crys/). The principal steps of the crystallization from our oriented but quiescent melt are sketched in Figure 6.

A semi–quantitative analysis of the nanostructure and its evolution for the different crystallization conditions from our experiments is presented in a following section.

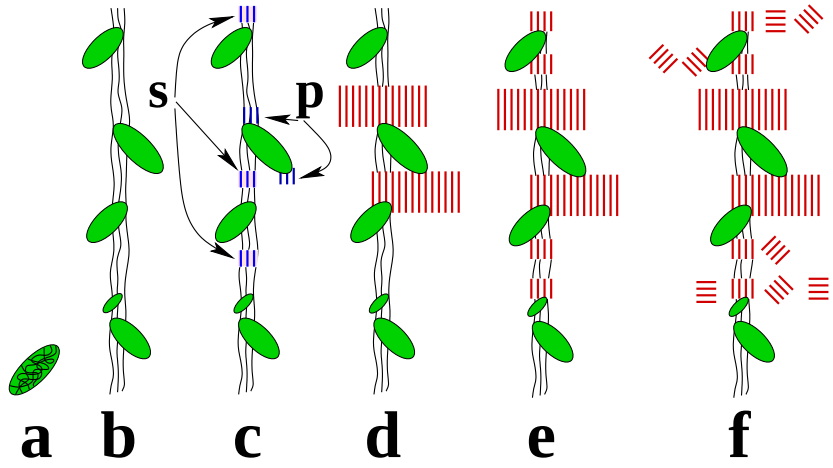

Figure 6: Sketch of the principal steps of crystallization from a highly oriented, quiescent polyethylene melt as indicated from CDF-images generated from 2D–SAXS/WAXS image series accumulated during a continuous, simultaneous in-situ experiment. Knots (entanglement strands, (a)) are represented in a simplified manner by ellipses. The backbone (b) is a sequence of bundles and knots, not an extended chain crystal. When crystallization starts (c), primary nuclei (p) induce a row of latent secondary nuclei (s) arranged on a lattice along the backbone. Primary crystallization (d) results in extended lamellae grown from the primary nuclei only. Secondary crystallization starts (e) with the generation of rows of blocks, followed by (f) the crowding of virtual planes oriented perpendicular to the fibre direction by unoriented, block-shaped crystals

5.3 The ultimate structure

Back at room temperature all samples show a two-component nanostructure made from both lamellae and blocks. The average lateral extension of the lamellae in the ultimate structure is lower (70 nm) than that observed directly after the beginning of the crystallization process (100 nm).

Figure 7 shows the different ultimate structures which are obtained as a result of different temperature programmes.

In the ultimate structure the longitudinal correlation peak (next strongest peak on the meridian) has changed its character. The peak that has been rather narrow when it has started to emerge (correlation between two blocks in fibre direction) has become a broad triangle. This observation does not indicate that blocks have merged to form lamellae, but only that there is no 3D colloidal lattice. On the other hand, a structured arrangement within a single plane filled with blocks is clearly indicated by the satellites to the strongest peaks (cf. arrows in Figure 7f). In our cursory study reported recently [22] we crystallized at 127°C, but found no longitudinal correlation among planes tiled with blocks. Instead, the longitudinal correlation was found to be restricted to rows of single blocks. From the former experiment we unfortunately have neither WAXS data nor data concerning the achieved structure of the annealed melt.

The shape of the satellites to the strongest peaks in the ultimate CDF is indicating the distribution of block sizes. Blocks are more uniform and bigger, if the material is quenched after isothermal crystallization (Figure 7c,e). As well a crystallization at a low temperature that is, in general, favouring the formation of blocks provides for more uniform blocks (compare Figure 7b with Figure 7a).

If we crystallize for half an hour at a very low temperature (120°C, Figure 7b), the ultimate nanostructure is no longer a function of the cooling rate chosen.

The samples which have not completely been

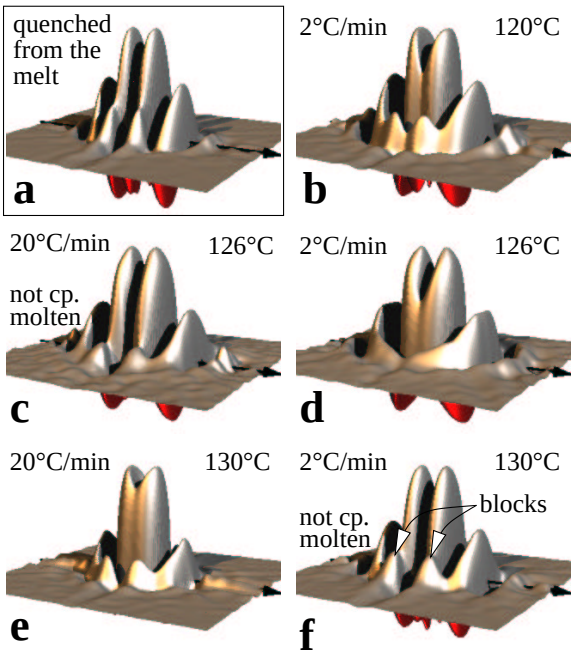

Figure 7: Oriented crystallization of PE from the melt. Ultimate nanostructures as revealed in the CDF. The images show the top view of the CDF in the range $|r_{12}|, |r_3| \leq 150\,\mathrm{nm}$. The r_3–direction (meridian) is indicated by an arrow in the base plane. Indicated are the crystallization parameters and, in addition, if the crystals were not completely molten during 2 min melt annealing at 140°C

molten (Figure 7a,c,f) exhibit their strongest peaks in the CDF extending on a straight line parallel to the equator. In contrast, the corresponding peaks of the samples which have been completely molten during melt-annealing (Figure 7b,d,e) exhibit arc-shaped positive peaks. As revealed in the movies generated from the stream of X-ray data, the bending is the result of preferential directed thickness growth of twin lamellae during the isothermal phase, away from the nuclei at the tips of the tilted entanglement strands. Thus the central part from the set of three triangles is moving outward (thickness growth), whereas the outer triangles (amorphous zone in between) remain at almost the same position. An explanation for the different behaviour of the two kinds of samples appears to be obvious. If the memory of the sample is not only in the knots of the cool melt, but as well in remnant crystallites, lamellae grow from these un-melted crystallites, and a considerable fraction of the original lamellae is instantly restored.

5.4 Semi-quantitative evaluation of the domain structure

A complete evaluation of the high-resolution multidimensional data from our experiments would require novel concepts for data evaluation as well as a multidimensional modelling of the data to be developed. We do not have the means to surmount this task in a reasonable period of time. Nevertheless, even at this stage we can acquire more in-depth notions concerning the structure transfer between the melt and the solid state, if only we study the positions of the peak maxima in the CDF. Moreover, the results obtained by such analysis may result in hints concerning the answer to the question of how to design more advanced methods of data analysis.

In any case, a shortcoming of this semi-quantitative analysis is that it can only be applied to such peaks in the CDF which are sufficiently separated from each other. Most clearly this is the case for the crystallization at 130°C. Here all the peaks that are of primary interest for the nanostructure are well-separated. For the materials crystallized at lower temperature this is no longer the case, and for analysis we have to pick clear peaks with a less direct meaning.

5.4.1 Isothermal crystallization at high temperature

Figure 8 shows the variation of nanostructure parameters as a function of time after quenching to 130°C as determined from the positions of the peak maxima in the CDF. Only a fraction of the collected images have been subjected to this analysis. Cooling rate during quenching is 20°C/min. Crystallization starts 35 s after leaving the melt-annealing temperature of 140°C. During the first 100 s the most probable thickness of the crys-

tallites in the ensemble (filled circles) is 24 nm. The most probable amorphous gap between twin lamellae (open circles) is rapidly decreasing from 30 nm to 23 nm. On this level it remains constant for 5 min. The most probable transversal offset of the crystalline lamellae from twins with respect to each other (diamonds) is initially continuously decreasing to 16 nm. Thereafter this parameter, as well, is constant for 5 min. During this first 5 min the stable crystalline domain is a fairly extended lamella (100 nm diameter). In the period between 2 min and 5 min we both observe a continuous increase of the most probable layer thickness to 27 nm and an increase of the crystal orientation in the WAXS pattern. During this period of crystallite thickness growth the distance between both the correlated lamellae is constant. Thus the semi-quantitative analysis now provides means to measure the phenomenon of directed thickness growth that has already been detected by inspection of the movies. In the image inset in Figure 8 the proposed average stabilising primary knot (entanglement strand) is indicated between the two lamellae.

After the first 5 min the generation of blocky crystals (secondary crystallization) is starting in addition to the continued formation of lamellae. The average transversal offset in twins is considerably decreasing, then becomes more and more diffuse, and cannot be determined any more for crystallization periods >20 min. The most probable crystalline thickness (as measured in fibre direction) is once again increasing up to a value of 30 nm, but here we can no longer address this phenomenon by the term layer thickness growth because — as is exhibited by the 2D WAXS data measured simultaneously [26] — the blocky crystals are oriented at random.

During the final quenching after an isothermal phase of 30 min the average crystal extension decreases considerably and the nanostructure becomes heterogeneous to such an extent that the determination of most of the nanostructure parameters becomes insignificant.

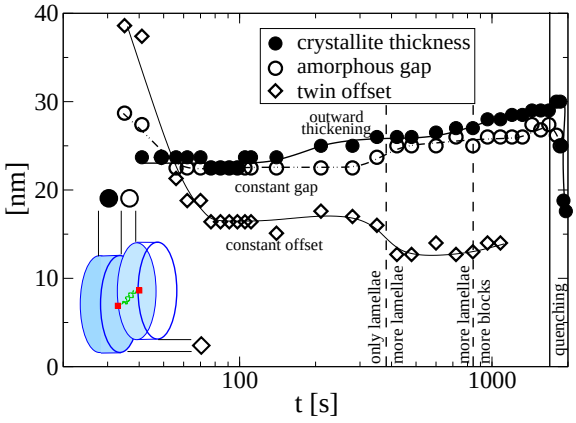

Figure 8: Isothermal crystallization at 130°C followed by quenching. Parameters of the nanostructure as determined from the maxima of the corresponding peaks in the CDF

5.4.2 Crystallization during quenching from the cool melt

Nanostructure is evolving in a different manner, if the material is cooled from the melt as fast as possible (20°C/min). Figure 9 presents the structural data retrieved from the peak maxima in the CDF. The first crystals are observed when the temperature has dropped to 130°C. Down to a temperature of 118°C we only observe the formation of lamellae; at lower temperatures blocky crystals are becoming predominant.

During the initial period the average layer thickness (filled circles) drops from 24 nm to 20 nm, where it pauses a while up to the time when the formation of blocky crystals is starting. Thereafter it decreases to 15 nm. The amorphous interlayers (open circles) and the transversal offset of twin lamellae (diamonds) are constantly high during the phase of layer generation. As soon as the formation of blocks is starting, the transversal offset cannot be determined any longer and the average amorphous thickness drops to the level of the extension of the secondary crystalline blocks. A longitudinal correlation (solid line) of blocks in the fibre direction is the first clear indication of block formation. Particularly distinct are the corresponding positive peaks on the positive face of the CDF. They characterise the distance from the

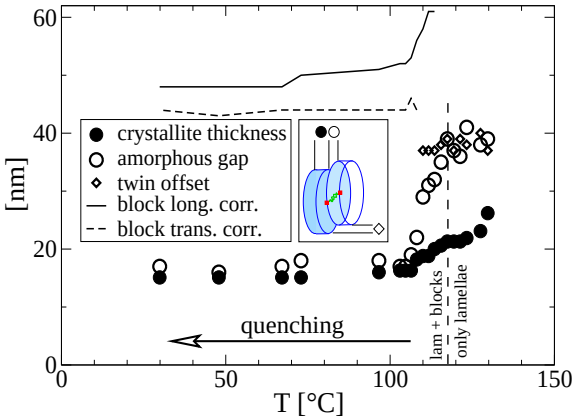

Figure 9: PE crystallization during the quenching (20°C/min) from the melt. Parameters of the nanostructure as determined from the maxima of the corresponding peaks in the CDF

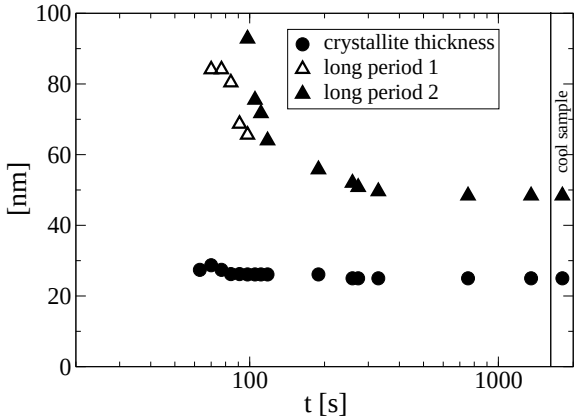

Figure 10: Isothermal crystallization at 126°C. Parameters of the nanostructure as determined from the maxima of the corresponding peaks in the CDF. The long periods are very weak during the first 10 min (little correlation among domains), and peak maxima of block arrangement cannot be determined

"upper" end of a block to the "lower" end of its neighbour. Thus the value determined from the peak position is $L + b$, long period plus block extension in fibre direction. The corresponding value (solid line) drops from initially 60 nm to 50 nm and then remains at this lower level. For temperatures below 110°C we as well find a transversal correlation among blocks (dashed line). According to the peak position the distance between neighbouring blocks in the (layer) plane is constant at 43 nm.

As expected, the average crystallite sizes are considerably smaller for the material that has been quenched from the melt as compared to the material discussed before (isothermally crystallized at a high temperature). Moreover, here there are less lamellae, and because of the quenching the block size distribution is relatively narrow. This causes the nanostructure made from arranged blocks to become particularly clear in the CDF of this material.

5.4.3 Isothermal crystallization at medium and low temperature

At medium (126°C) and low (120°C) crystallization temperature the semi-quantitative data analysis is more difficult than in the two cases discussed before, because a superposition of lamellar and block structure is observed almost from the beginning of the isothermal phase.

Thus during crystallization at 126°C (Figure 10) a slow decrease of the most probable crystallite thickness (filled circles) from 24 nm to 20 nm is observed, and the only other parameter that is easily accessible is the long period. At the beginning of crystallization two clear long periods (triangles) are found in the CDF, which merge 2 min after the quenching. In the beginning the long period is rapidly decreasing and indicates a predominantly statistical process of crystallite placing in the volume ("random car parking" [23]). Only 5 min after the quenching the most probable structural parameters have reached their ultimate value. They even do not change during the quenching after the isothermal phase. From both the data accumulated at the ESRF and the earlier data from the cursory study at HASYLAB [22] we estimate the same lateral distance between two blocks from the same plane (45 nm).

If the melt is crystallized at 120°C (Figure 11), the decrease of the crystallite thickness from 24 nm to 20 nm is much faster than in the material crystallized at 126°C. After only 2 min the satellite peaks of blocks arranged in planes (open triangles) are very clear. Initially the distance of

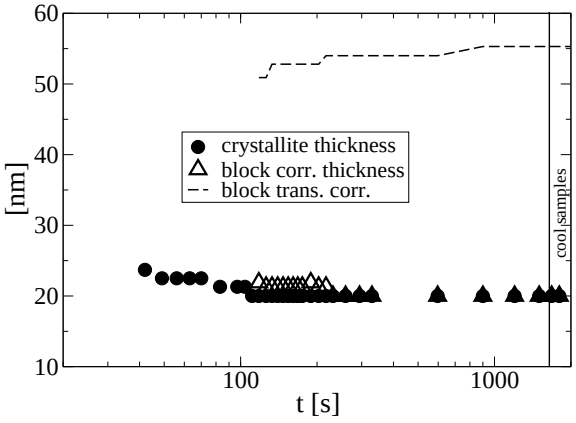

Figure 11: Isothermal crystallization at 120°C. Parameters of the nanostructure as determined from the maxima of the corresponding peaks in the CDF

the satellite peaks from the equator is somewhat longer than that of the central peak. This means that the extensions in fibre direction of the blocks arranged in planes are somewhat thicker than the most probable thickness of all crystallites. The reason may be the random orientation of crystal axes in the blocks. 4 min after the start of the crystallization there is no more difference.

While the long period is decreasing during crystallization, the average transverse distance between neighbouring blocks in a plane (dashed line) is slightly increasing from 50 nm to 55 nm. As well at this low crystallization temperature, the final cooling to ambient temperature has no effect on the average parameters of the nanostructure. Here, at the lowest crystallization temperature chosen, even the widths of the peaks and thus the widths of the distributions of the nanostructure parameters are neither changed by cooling nor by variation of the cooling rate.

6 Conclusions

In this paper we have shown that the analysis of X-ray data from polymer materials recorded with high resolution in time and space can be carried out in physical space. It results in a detailed, almost continuous data stream which reflects the evolution of nanostructure during materials processing. By application of this method we have been able to gain a rather detailed description and notion concerning the mechanisms that control the formation of crystals in our oriented polyethylene melt.

After a semi-quantitative analysis we, moreover have obtained curves describing the variation of nanostructure parameters during the crystallization processes investigated. We expect that similar studies will contribute to the understanding of the relationships between process control parameters and the features of the resulting nanostructure, in particular if the typical industrial production stages with respect to polymer materials processing like fibre spinning, extrusion, straining or annealing are set up at a modern synchrotron beam line, monitored continuously by 2D detectors, and finally analysed by advanced data evaluation procedures that incorporate the fields of scattering theory and digital image processing.

Even if the novel combination of experiment and analysis provides detailed insight into the mechanisms of nanostructure transfer, new limits of cognition become apparent. For example, we now would wish to be able to discriminate the continued growth of “early” crystals from the effects arising from the formation and growth of late crystals. In order to perform such investigations it would be desirable to minimise the volume integration of the scattering method down to a cross-section far below that of the presently available microfocus beams, or to advance an imaging method in a way that it can be used in-situ in a minimal invasive environment, similar to what already at this stage can be achieved by utilisation of X-rays.

Acknowledgement. We thank the European Synchrotron Radiation Facility, Grenoble, for beam time granted in the frame of project SC 1396.

References

[1] Heck B, Hugel T, Iijima M, Sadiku E, Strobl G (1999) New J Phys 1:17.1

[2] Heck B, Hugel T, Iijima M, Strobl G (2000) Polymer 41:8839

[3] Heeley EL, Maidens AV, Olmsted PD, Bras W, Dolbnya IP, Fairclough JPA, Terrill NJ, Ryan AJ (2003) Macromolecules 36:3656

[4] Bras W, Dolbnya I, Detollenaere D, van Tol R, Malfois M, Greaves G, Ryan A, Heeley E (2003) J Appl Cryst 36:791

[5] Somani RH, Yang L, Hsiao BH, Fruitwala H (2003) J Macromol Sci Part B Phys B42:515

[6] Somani RH, Yang L, Hsiao BS, Agarwal PK, Fruitwala HA, Tsou AH (2002) Macromolecules 35:9096

[7] Yamazaki S, Hikosaka M, Toda A, Wataoka I, Yamada K, Tagashira K (2003) J Macromol Sci Part B Physics B42:499

[8] Allegra G, Meille SV (1999) Phys Chem Chem Phys 1:5179

[9] Pearce R, Vancso GJ (1998) Polymer 39:1237

[10] Hobbs JK, Humphris ADL, Miles MJ (2001) Macromolecules 34:5508

[11] Humphris ADL, Hobbs JK, Miles MJ (2003) Appl Phys Lett 83:6

[12] Stribeck N (1993) Colloid Polym Sci 271:1007

[13] Stribeck N (2000) ACS Symp Ser 739:41

[14] Stribeck N (2001) J Appl Cryst 34:496

[15] Stribeck N (2002) Colloid Polym Sci 280:254

[16] Ruland W (1971) J Appl Cryst 4:70

[17] Perret R, Ruland W (1971) Colloid Polym Sci 247:835

[18] Brämer R, Ruland W (1976) Makromol Chem 177:3601

[19] Ruland W (1977) Colloid Polym Sci 255:417

[20] Ruland W (1977) Colloid Polym Sci 255:833

[21] Ruland W (1987) Macromolecules 20:87

[22] Stribeck N, Almendarez Camarillo A, Cunis S, Bayer RK, Gehrke R (2004) Macromol Chem Phys 205:1445

[23] Stribeck N (2004) Macromol Chem Phys 205:1455

[24] Stribeck N, Almendarez Camarillo A, Bayer R (2004) Macromol Chem Phys 205:1463

[25] Barham PJ, Keller A (1985) J Mater Sci 20:2281

[26] Stribeck N, Bayer R, Bösecke P, Almendarez Camarillo A (2004) Polymer in print

[27] Stribeck N, Buzdugan E, Ghioca P, Serban S, Gehrke R (2002) Macromol Chem Phys 203:636

[28] Stribeck N, Funari SS (2003) J Polym Sci Part B Polym Phys 41:1947

[29] Bayer RK (1991) Colloid Polym Sci 269:421

[30] Bayer RK, Liebentraut F, Meyer T (1992) Colloid Polym Sci 270:331

[31] Bayer RK (1994) Colloid Polym Sci 272:910

[32] Stribeck N, Bayer R, von Krosigk G, Gehrke R (2002) Polymer 43:3779

[33] Narayanan T, Diat O, Bösecke P (2001) Nucl Instrum Methods Phys Res Sect A 467-468:1005

[34] Bösecke P, Diat O (1997) J Appl Cryst 30:867

[35] Urban V, Panine P, Ponchut C, Bösecke P, Narayanan T (2001) J Appl Cryst 36:809

[36] pv-wave, version 7.5 (2001), Visual Numerics Inc., Boulder, Colorado

[37] Vonk CG (1979) Colloid Polym Sci 257:1021

[38] Rosenfeld A, Kak AC (1982) Digital Picture Processing, vol. 1. Academic Press, London

[39] Haberäcker P (1989) Digitale Bildverarbeitung. Hanser, Munich